ultrasound systems. Am J Card Imaging 1996;10:209-218.

17. Hiro T, Leung CY, De Guzman S, et al. Are soft echoes really soft? Intravascular ultrasound assessment of mechanical properties in human atherosclerotic tissue. Am Heart J 1997;133:1-7.

18. Kimura BJ, Bhargava V, DeMaria AN. Value and limitations of intravascular ultrasound imaging in characterizing coronary atherosclerotic plaque. Am Heart J 1995;130:386-396.

19. Jeremias A, Kolz ML, Ikonen TS, et al. Feasibility of in vivo intravascular ultrasound tissue characterization in the detection of early vascular transplant rejection. Circulation 1999;100:2127-2130.

20. Bridal SL, Fornes P, Bruneval P, et al. Parametric (integrated backscatter and attenuation) images constructed using backscattered radio frequency signals (25-56 MHz) from human aortae in vitro. Ultrasound Med Biol 1997;23:215-229.

21. Linker DT, Yock PG, Gronningsaether A, et al. Analysis of backscattered ultrasound from normal and diseased arterial wall. Int J Card Imaging 1989;4:177-185.

22. Kawasaki M, Takatsu H, Noda T, et al. Non-invasive tissue characterization of human atherosclerotic lesions in carotid and femoral arteries by ultrasound integrated backscatter: comparison between histology and integrated backscatter images before and after death. J Am Coll Cardiol 2001; 38:486–492.

23 Kawasaki M, Takatsu H, Noda T, et al. In Vivo quantitative tissue characterization of human coronary arterial plaques by use of integrated backscatter intravascular ultrasound and comparison with angioscopic findings. Circulation

2002 ;105:2487-2492.

24. Wilson LS, Neale ML, Talhami HE, et al. Preliminary results from attenuation-slope mapping of plaque using intravascular ultrasound. Ultrasound Med Biol 1994;20:529-542.

25. Daubechies I, Grossmann A. An integral transform related to quantization. J Mat Phys 1980;21:2080-2090.

26. Benkeser PJ, Churchwell AL, Lee C, et al. Resolution limitations in intravascular ultrasound imaging. J Am Soc Echocardiogr 1993;6:158-165.

27. Nair A, Kuban BD, Tuzcu EM, et al. Coronary plaque classification with intravascular ultrasound radiofrequency data analysis. Circulation 2002;106:2200-2206.

28. de Korte CL, Sierevogel MJ, Mastik F, et al. Identification of atherosclerotic plaque components with intravascular ultrasound elastography in vivo: a Yucatan pig study. Circulation 2002;105:1627-1630.

29. Hiro T, Fujii T, Yasumoto K, et al. Detection of fibrous cap in atherosclerotic plaque by intravascular ultrasound by use of color mapping of angle-dependent echo-intensity variation. Circulation 2001;103:1206-1211.

FIGURE LEGENDS

Figure 1. Acquisition of RF IVUS Signals.

There are 256 radial vectors of RF signal sampled around the IVUS catheter.

Figure 2. Procedure of Wavelet analysis.

In this example, a wavelet is stretched twice and three times. At a time of t0, a high value of wavelet coefficient is provided (arrow). This suggests that a special wave pattern similar to the wavelet of scale 2 is included within the signal at the time.

Figure 3. Representative examples of in vitro Wavelet analysis of RF IVUS signals from a lipid-laden plaque (A) and from a fibrous plaque without a lipid core (B). The upper panel shows RF signals, the middle panel, the results of Wavelet analysis, the lower panel, histologic specimen of the corresponding arterial cross-section with Masson's trichrome. In the time-scale domain color-coded mapping of Wavelet analysis, a apparently different pattern of pink area from a RF signal vector of a lipid-laden plaque is observed between scale 20 and scale 30, compared to the fibrous plaque. F: Fibrous area, L: lipid core.

Figure 4. ROC analysis

ROC analysis was performed with varying degree of the wavelet coefficient in terms of the capability of the in vitro detection of lipid-laden plaque. This analysis revealed that

the optimal value of this wavelet coefficient in order to discriminate a lipid-laden plaque was 0.6.

C: the wavelet coefficient.

Figure 5. Representative examples of in vivo Wavelet analysis of RF IVUS signals from a lipid-laden plaque (A) and from a fibrous plaque without a lipid core (B). The left panel shows conventional IVUS images, the middle panel, the results of Wavelet analysis, the right panel, histologic cross section of the corresponding DCA specimen with Hematoxylin-Eosin and Azan stains. A similar pattern of color mapping was observed from the RF signal vector of a lipid-laden plaque as seen in the in vitro study.

Figure 1

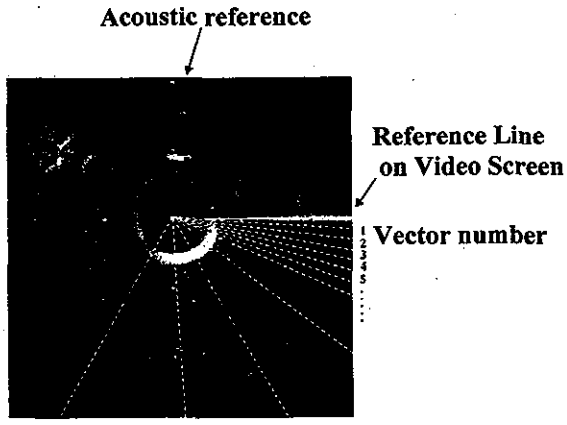
Acoustic reference
Reference Line
on Video Screen
Vector number

Figure 2

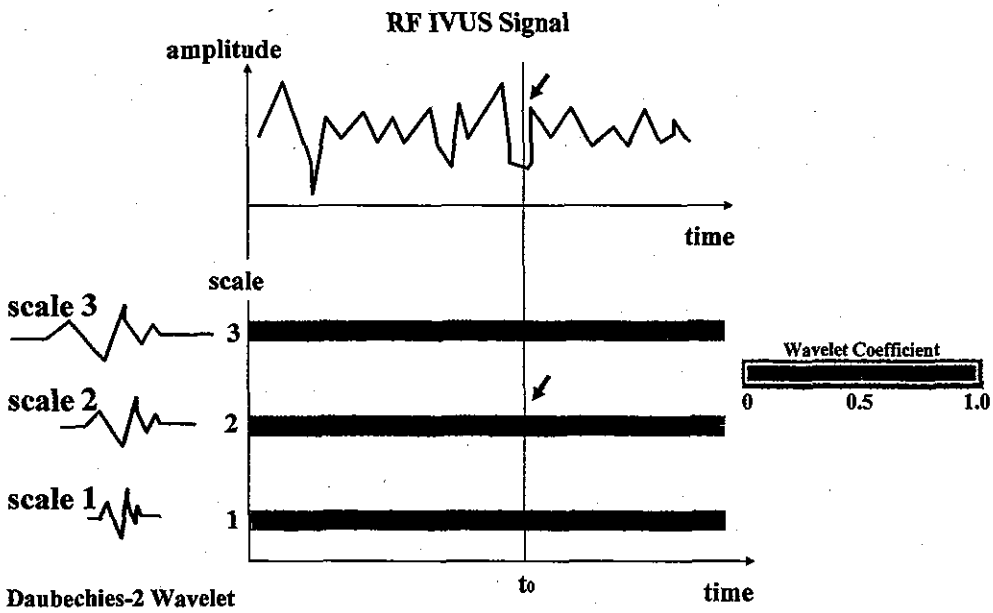
RF IVUS Signal
amplitude
time
scale
scale 3
3
scale 2
2
scale 1
1
Wavelet Coefficient
0
0.5
1.0
Daubechies-2 Wavelet
to
time

Figure 3

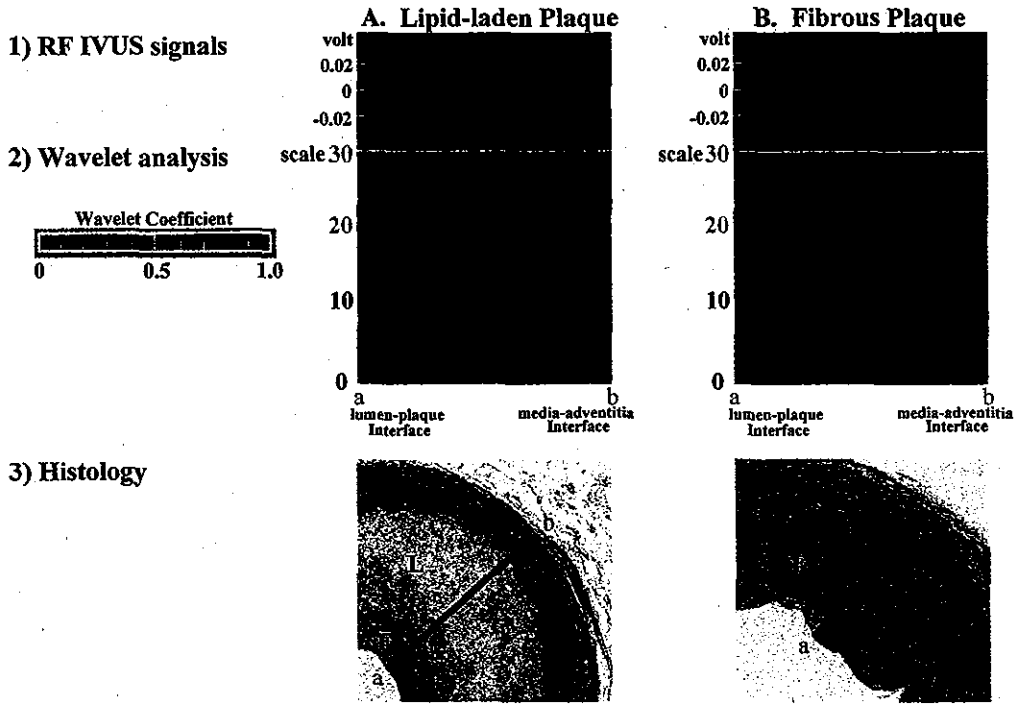
1) RF IVUS signals
2) Wavelet analysis
Wavelet Coefficient
0
0.5
1.0
3) Histology
A. Lipid-laden Plaque
B. Fibrous Plaque
volt
0.02
0
-0.02
scale 30
20
10
0
a
lumen-plaque Interface
b
media-adventitia Interface
L
a
b

Figure 4

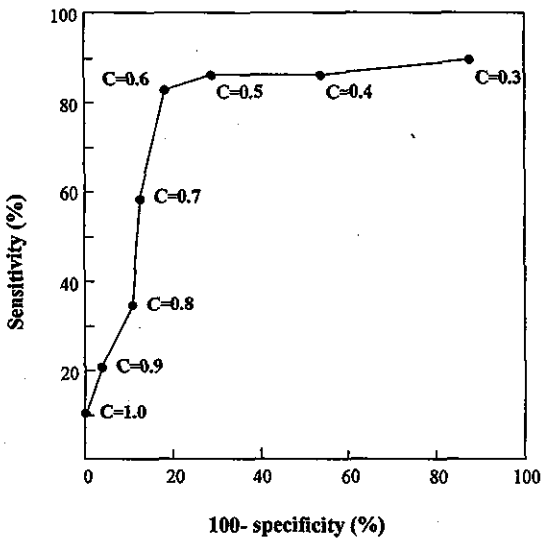
100
80
60
40
20
0
20
40
60
80
100
C=0.6
C=0.5
C=0.4
C=0.3
C=0.7
C=0.8
C=0.9
C=1.0
Sensitivity (%)
100- specificity (%)

Figure 5

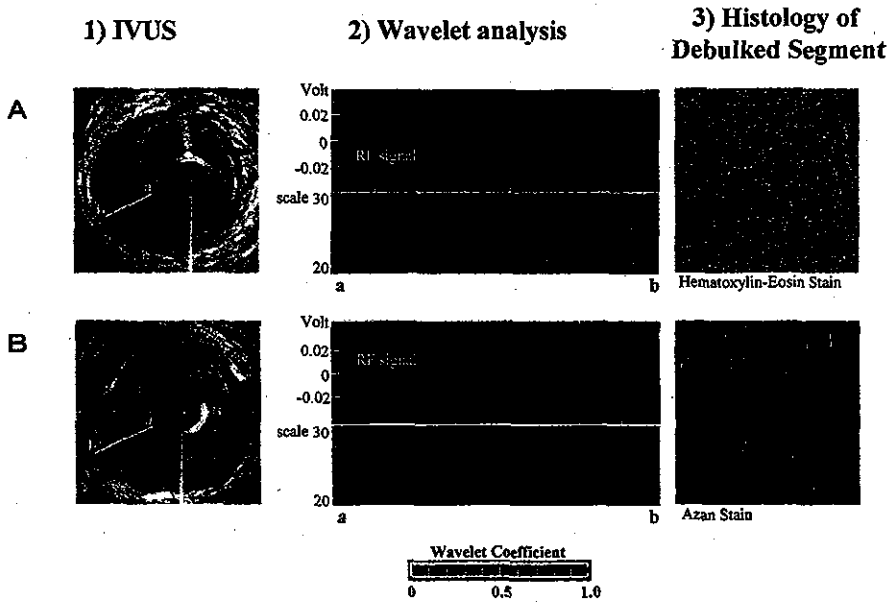
1) IVUS
2) Wavelet analysis
3) Histology of Debulked Segment
A
B
Volt
0.02
0
-0.02
scale 30
20
a
b
Hematoxylin-Eosin Stain
Azan Stain
Wavelet Coefficient
0
0.5
1.0

Table 1. Sensitivity and Specificity of Wavelet Analysis of RF IVUS Signals for Detecting Lipid-laden Plaque

Histology		Wavelet Coefficient	
		≧0.6	<0.6
Lipid core (+)	In Vitro (n=29)	24/29(83%)	5/29(17 %)
	In Vivo (n=16)	13/16(81%)	3/16(19 %)
Lipid core (-)	In Vitro (n=56)	10/56(18%)	46/56(82%)
	In Vivo (n=13)	2/13(15%)	11/13(85%)